International Journal of Biological Macromolecules 163 (2020) 2248–2258

Contents lists available at ScienceDirect

International Journal of Biological Macromolecules

journal homepage: http://www.elsevier.com/locate/ijbiomac

The assessment of antibiofilm activity of chitosan-zinc oxide-gentamicin nanocomposite on *Pseudomonas aeruginosa* and *Staphylococcus aureus*

Fatemeh Hemmati [a,d], Roya Salehi [b], Reza Ghotaslou [c], Hossein Samadi Kafil [b,c], Alka Hasani [c], Pourya Gholizadeh [a,d], Mohammad Ahangarzadeh Rezaee [a,c,*]

[a] Immunology Research Center, Tabriz University of Medical Sciences, Tabriz, Iran
[b] Drug Applied Research Center, Tabriz University of Medical Science, Tabriz, Iran
[c] Department of Medical Microbiology, Faculty of Medicine, Tabriz University of Medical Sciences, Tabriz, Iran
[d] Student Research Committee, Tabriz University of Medical Sciences, Tabriz, Iran

ARTICLE INFO

Article history:
Received 22 June 2020
Received in revised form 17 August 2020
Accepted 7 September 2020
Available online 11 September 2020

Keywords:
Antimicrobial agents
Chitosan
Gentamicin
Nanocomposite
Zinc oxide

ABSTRACT

In the present study, chitosan-zinc oxide (CS-ZnO) nanocomposite with/without gentamicin was synthesized and characterized which used as an antibiofilm agent to inhibit the biofilm formation of *Pseudomonas aeruginosa* (*P. aeruginosa*) PAO1 and *Staphylococcus aureus* (*S. aureus*). Synthesized CS-ZnO nanocomposite was characterized with the DLS (Dynamic Light Scattering), FTIR (Fourier Transform Infrared), XRD (X-ray Diffraction) and SEM (Scanning Electron Microscope). The minimum inhibitory concentrations (MICs) against *P. aeruginosa* PAO1 and *S. aureus* determined using broth microdilution methods. The influence of sub-MIC (1/4 MIC) and MIC concentration of CS-ZnO nanocomposite and gentamicin alone and in combination on biofilm formation was also determined. A four-fold MIC reduction in *S. aureus* and *P. aeruginosa* PAO1 treated by the gentamicin loaded CS-ZnO nanocomposite, and 84% reduction of biofilm formation for *P. aeruginosa* PAO1 and 77% reduction of biofilm formation for *S. aureus*, was observed compared to the gentamicin alone ($P < 0.05$).
This study showed the important role of nanocomposite in designing novel antibacterial and antibiofilm agents to combat the *P. aeruginosa* and *S. aureus* biofilm-related infections.

1. Introduction

The excessive use of antibiotics to fight bacterial infections caused the increased bacterial resistance to multiple antibiotics [1]. The resistance is due not only to the uncontrolled use of antibiotics, but also to the fact that pathogenic bacteria are capable of adapting to various environments and develop self-defense strategies such as survival in biofilms [2]. In general, the biofilms are comprised of the microbial communities which protected with the extracellular polymeric matrix [3]. The attendance of biofilm increases bacteria resistance to conventional antibiotics with up to 1000-fold compared to their planktonic (free-living) equivalents. Biofilms are responsible for around 60% to 85% of human bacterial infections [1,4]. Biofilm-related infections are drastically decreased susceptibility to conventional antibiotics, and these are hard to eradicate with antibiotic therapy alone [5].

During the last decades, many efforts were taken to develop ecologically-friendly and low cost, natural or synthetic substances as treatment agents [1]. The incidence of acute infections of antibiotic and/or multidrug-resistant bacteria at a worrying rate caused several researches interest to evaluate the antibacterial and antibiofilm activities of different substances [4].

Chitosan (CS) is considered a medically significant material due to its unique properties such as biocompatibility, biological activity, nontoxicity, bioadhesion, antioxidant, antibiofilm, and antimicrobial activities [6,7]. CS is an abundant natural polysaccharide biopolymer, widely used in the medical field [8]. The antibacterial and antibiofilm properties of CS are due to the presence of its positive charge amino groups which cause a reaction with bacterial membrane [8,9]. Furthermore, CS with vast surface areas modifies the bacterial membrane penetrability via the membrane incorporation and leads to bacteria's death [10,11].

Zinc oxide (ZnO) is another material which received more attention due to its antibacterial and antibiofilm activities against a wide range of bacteria [12]. ZnO has revealed great against bacteria pathogens by generating the reactive oxygen species (ROS) and decreasing membrane structure integrity [13]. Green production of ZnO NPs has been done via various plant extracts, for example, *Cassia fistula*, *Ocimum*, *Trifolium pratense* [14] and *Rosa canina* [15]. *Rosa canina* is a medicinal plant related to family *Rosaceae*. Rosehip or the small fruit of *Rosa canina* is recognized for its high content of vitamin C. Furthermore, the rosehip has a

* Corresponding author at: Immunology Research Center, Faculty of Medicine, Tabriz University of Medical Sciences, Tabriz, Iran.
E-mail address: rezaee.mohammad@gmail.com (M.A. Rezaee).

https://doi.org/10.1016/j.ijbiomac.2020.09.037
0141-8130/

high level of antioxidants such as flavonoids and phenolic compounds. Due to the reports, rosehip possesses preventive and curative activity against a broad range of diseases such as renal, inflammatory, gout, and gastric disorders [16]. The preparation of NPs using plant extract is a new technique which is a low-cost and eco-friendly process [14]. ZnO can be combined with other nanomaterial or antibiotics to develop antibacterial and antibiofilm properties and less toxicity for human cells [17].

CS can be used as supportive material for metal NPs [18]. CS-ZnO (CS-ZnO) nanocomposite is obtained from the incorporation of ZnO into the CS NPs [19]. CS-ZnO nanocomposites can become a strong antibacterial and antibiofilm agents due to the co-employment of antibacterial activities of CS and ZnO NPs [1]. Several researches suggested the synthetic compounds in combination with antibiotics to control antibiotic-resistant bacteria [17,19,20].

The gentamicin related to aminoglycoside antibiotics family is widely used to treat several hospital-acquired infections. These antibiotics were effectively used against Gram-negative [21]. The gentamicin is bacteriocidal and its mode of action by preventing normal protein synthesis by linking it to the highly-conserved A-site of bacterial 16S subunit of 30S rRNA [22]. This binding leads to the distraction of proofreading in the protein synthesis process; as a result, bacterial virulence factors production, including biofilm, can be disturbed [23,24].

Moreover, the incidence of serious infections caused by bacteria's biofilm in an alarming level which prompted many researches to explore the antibiofilm activities of different materials [4,25]. Therefore, we evaluated the effect of CS and ZnO NPs and CS-ZnO nanocomposite with/without gentamicin on biofilm formation of *P. aeruginosa* PAO1 and *S. aureus*.

2. Materials and methods

2.1. Experimental procedure

2.1.1. Materials

CS (molecular weight 50–190 kDa, DA ≥ 75), sodium tripolyphosphate (TPP), gentamicin stock solutions (10 mg/mL) and zinc nitrate hexahydrate $Zn(NO_3)_2 \cdot 6H_2O$ with 98% purity was bought from Sigma-Aldrich, Mueller Hinton agar/broth (Merck, Germany), Tripticase soy broth (Merck, Germany) and strains of *P. aeruginosa* PAO1 and *S. aureus* ATTC25923.

2.1.2. Preparation of chitosan nanoparticles

CS NPs were created with the ionic crosslinking of CS with TPP, as previously described [26,27]. In brief, about 0.1% CS solution was prepared in a 1% acidic solution, and a 1% TPP solution was prepared in deionized water. NPs were produced by dropwise addition of 1 mL of prepared TPP solution into 10 mL CS solution under stirring at 4 °C temperature about 30 min. The formed NPs were separated with the centrifugation at 12,000 rpm for 45 min they were washed twice with deionized water and lyophilized.

2.1.3. Preparation of ZnO nanoparticles

The pure ZnO NPs were synthesized with the fruit extract of *Rosa canina*, as previously described [15]. For the preparation of extract, harvested *Rosa canina* fruits were washed with deionized water and retained in shading to dry. The flesh of the fruits was cautiously powdered and weighted. About 10 g of powder was dispersed in 100 mL deionized water, ultrasonicated for 30 min three times, and incubated in the oven at 60 °C for 10 min. The rose-color of mixture demonstrated that the extraction had happened. To get pure product, the mixture sieved, centrifuged, and lastly preserved in refrigerator at 180 °C for additional experiments.

ZnO NPs were synthesized by the conventional heating (CH) technique. For this purpose, 5 mL of 0.05 M zinc nitrate solution was added into 10 mL of prepared *Rosa canina* extract. The final pH was adjusted at 6.0 by adding 1 N NaOH solution. The solution was held under severe stirring at 150 °C for an additional 5 h until a change of color happens. After cooling at room temperature, it was centrifuged at 5000 rpm for 10 min, and solid sediment was attained. The sediment was washed twice with the deionized water and dried at 60 °C for 5 h. This sediment was heated in a furnace at 400 °C for 4 h. At last, the solid white product was attained that was completely powdered using a mortar.

2.1.4. Preparation of chitosan-zinc oxide nanocomposite

CS-ZnO nanocomposite was synthesized by dispersing 1.0 g ZnO powder in 100 mL of 1% acetic acid solution to get zinc cations. 1.0 g of CS was added in the solution and ultrasonicated for 15 min. Freshly prepared 1 N NaOH solution was added dropwise to bring pH 10. The solution was incubated in the water bath for 3 h at 60 °C. After cooling at room temperature, it was filtered, and a white precipitate was found which was washed twice with deionized water and dried at 60 °C [28].

2.1.5. Preparation of gentamicin coated nanoparticles

To prepare the gentamicin loaded CS and ZnO NPs, the method described by Voicu et al. [20] was used. The fresh-prepared NPs (0.06 g) was dispersed in 10 mL gentamicin 1% acidic solution (10 mg/mL), ultrasonicated for 30 min, and held under stirring at room temperature for 24 h. After the centrifugation, the supernatant solution was discarded, and precipitate of NPs coated with gentamicin was dried. To prepare gentamicin loaded CS-ZnO, the method described by Vasile et al. [19] was used. In brief, 0.1 g ZnO was dispersed in 5 mL gentamicin solution (0.03 g gentamicin). Then, 5 mL aqueous solution comprising ZnO-gentamicin nanopowder was added to 10 mL of 1% acidic solution of CS (0.1 g) under magnetic stirring at room temperature few minutes. The CS-ZnO-gentamicin nanopowders were found by drying the gel.

2.2. Experimental techniques

2.2.1. Particle size distribution and zeta potential measurements

Size (*Z*-average mean) and zeta potential of the NPs was analyzed by Dynamic Light Scattering (DLS) method using Malvern Zetasizer (Malvern Instruments Ltd., UK) at a scattering angle of 135° at ambient temperature (25 ± 3 °C).

2.2.2. Electron microscope images

The scanning electron microscopy tests were done by FESEM (FEI Nova NanoSEM 450, USA, and MIRA3 TESCAN-XMU, USA) to investigate the size and the morphology of synthesized NPs.

2.2.3. X-ray diffraction

X-ray powder diffraction patterns were found with an XRD diffractometer (Kristalloflex D500, Siemens, Germany). The powders were exposed to Cu Kα radiation at 40 kV, current of 40 mA and wavelength of 1.540 Å within the diffraction angles (2θ) of range 5–75° at room temperature. A scan rate of 1° min^{-1} was employed.

2.2.4. Fourier transform infrared spectroscopy

Fourier transform infrared (FTIR) spectra were determined using the KBr pellet method on an infrared spectroscopy (Tensor 27, Bruker, Germany) within the 400–4000 cm^{-1} frequency range. A total of 30 scans and a resolution of 1 cm^{-1} were employed in receiving the spectra.

2.2.5. Standard curve of gentamicin

The gentamicin samples were prepared in PBS solution (pH = 7.4) in the various concentrations (30, 40, 50, 60, 70, 80 and 90 μg/mL). 10 mL of assay samples were blended with 0.1 mL of freshly prepared ninhydrin reagent 1.25% (w/v) and incubated in a water bath at 95 °C for 5 min. The tubes were then cooled in an ice-water bath, and each

solution's absorption at 400 nm was recorded using a UV spectrophotometer. The gentamicin standard curve was drawn, and the corresponding data was regressed as standard equation [29].

2.2.6. Drug Loading

The drug entrapment efficiency of NPs was specified by separating the NPs from the aqueous medium containing non-loaded drugs with the centrifugation at 12,000 rpm for 30 min. The absorption of free gentamicin in the supernatant was recorded with the UV at 400 nm, and the amount of gentamicin was calculated due to the above standard curve. The gentamicin entrapment efficiency of NPs was calculated with recording the absorption of unbound gentamicin at 400 nm using the formula [30,31]:

$$\text{Drug entrapment } (\%) = \frac{\text{Total gentamicin–Free gentamicin}}{\text{Total gentamicin}} \times 100$$

2.2.7. Drug release

The gentamicin release was photometrically assessed using UV-spectrophotometer. The gentamicin release tests were done with immersing the samples (20 mg) in 10 mL PBS (pH: 7.4) in static conditions (120 rpm) at 37 °C for up to 24 h. At the determined times (0, 15, 30 min, 1, 2, 4, 6, 12 h), 300 μL aliquot was collected from supernatant of samples, centrifuged at 12,000 rpm for 5 min and evaluated using UV-spectrophotometer after interaction with ninhydrin as described at Section 3.5. Then, the percentage of gentamicin release was calculated with considering the specification of its absorbance peak at 400 nm. These data were compared to a calibration curve obtained from UV absorbance amount at 400 nm of a series of gentamicin concentrations. The tests were performed in triplicate and the results were reported as a mean [32].

2.2.8. Qualitative assay of the antimicrobial activity

The qualitative assay was carried out with disc diffusion method. The overnight culture of bacteria suspensions was adjusted to 0.5 McFarland standards and was used to inoculate onto plates containing Mueller Hinton (MH) agar medium. Filter papers (Φ 9 mm, pore size 0.45 μm) saturated with 20 μL of stock solution of each NPs were placed in the center of MH agar plates (stock solution = 10 mg/mL). The negative (blank disc) and positive controls (antibiotic stock solution-gentamicin 20 μg/mL) was used. After incubation of plates for 18–24 h at 37 °C, the inhibition zones' diameter was reported in mm. The tests were carried out in triplicate, and the results were reported as a mean ± standard deviation [19,20].

2.2.9. Quantitative assay of the antimicrobial activity

The Minimum Inhibitory Concentrations (MICs) values of tested chemical compounds were evaluated with the microdilution method, in polystyrene 96-well microplate, two-fold serial dilutions of CS NPs, ZnO NPs and CS-ZnO nanocomposite (2048, 1024, 512, 256, 128, 64, 32 and 16 μg/mL) and gentamicin and CS NPs, ZnO NPs and CS-ZnO nanocomposite combination with gentamicin (128, 64, 32, 16, 8, 4, 2, 1, 0.5, 0.25 and 0.125 μg/mL) was prepared. In brief, 100 μL sterile MH broth were distributed in sterile 96 well plates, and serial dilutions of each chemical compound were added in the wells. The overnight culture of bacteria was adjusted to 10^5 CFU/mL in wells. MH and MH broths involving the bacterial inoculum were considered as negative and positive controls, respectively. The plates were incubated for 18–24 h at 37 °C. After the incubation period, MIC was determined as the lowest concentration of tested chemical compounds which inhibited the visible growth of bacteria. The tests were carried out in triplicate, and the results were reported as a mean ± standard deviation [33].

2.2.10. Biofilm formation

The biofilm formation was measured in a polystyrene 96-well microplate. The overnight culture of bacteria strains was incubated for 24 h at 37 °C in Tryptic Soy Broth (TSB) containing 1% glucose in the absence and presence of 1/4 MIC and MIC concentrations of chemical compounds. The medium was removed; wells involving biofilms were washed twice with normal saline and were fixed with 150 μL of 99% methanol. The microplate dried at room temperature, and the wells were stained with 200 mL of 0.1% crystal violet for 15 min, washed twice with distilled water, and dried at room temperature. Then, dye attached to biofilm was solubilized with 200 mL of 33% glacial acetic acid, and the absorbance was recorded at 570 nm. The experiments were performed in triplicate and the results were reported as absorption means [34].

$$\text{Percentage of biofilm inhibition } (\%) = \frac{\text{Control OD} - \text{Test OD}}{\text{Control OD}} \times 100$$

2.2.11. Cytotoxicity studies

The cytotoxicity of CS-ZnO nanocomposite was evaluated by the MTT assay. Human fetal skin fibroblasts (HFFF2) cultured in Dulbecco modified Eagle medium (DMEM, high glucose formulation; Gibco BRL) supplemented with 10% (v/v) fetal bovine serum were seeded in triplicate into 96-well plates at a density of 1×10^4 cells/well. The cells were exposed by two different concentrations of CS-ZnO nanocomposite, including 128 and 64 μg/mL. All exposed cells were incubated for 24–48 h at 37 °C under 5% CO2. Afterward, 200 μL of new medium containing MTT solution (5 mg/mL) was replaced in each well and incubated for 3 h at 37 °C.

The MTT solution was cautiously removed, and 200 μL of dimethyl sulfoxide (DMSO) was added to dissolve the formazan crystals in each well. The absorption of solubilized formazan was recorded at 570 nm with a microplate reader (BioTeck, Bad Friedrichshall, Germany). The cells without NPs were considered as a control group. The viability of cells was calculated with following formula [15,35]:

$$\text{Viability of cells } (\%) = \frac{\text{Mean absorbance of each group}}{\text{Mean absorbance of control group}} \times 100$$

2.3. Statistical analysis

Statistical analyses were evaluated using GraphPad Prism vs. 8 software program. Statistical significance was tested by One-way ANOVA analysis and P-value < 0.05 was considered as significant.

3. Results

3.1. Size and zeta potential of synthesized nanoparticles

The size distributions of each NP were analyzed with the dynamic light scattering (DLS) method. The mean diameter of CS NPs, ZnO NPs and CS-ZnO nanocomposite were 60.3, 243.7, and 277.5 nm, respectively. After loading gentamicin to CS NPs, ZnO NPs and CS-ZnO nanocomposite, their size were changed to 63.1, 251.5 and 284.5 nm (Fig. 1). The zeta potential indicates the charge of a particle related to surrounding circumstances. The surfaces of CS and ZnO NPs have positive and negative charges, respectively. Zeta potential of CS NPs, ZnO NPs and CS-ZnO nanocomposite was 24.6, −18.2, and 14.7 mV, respectively. After loading gentamicin to CS NPs, ZnO NPs and CS-ZnO nanocomposite, their zeta potential were changed to 39.7, −12.8, and 29.4 mV, respectively, as shown in Fig. 2.

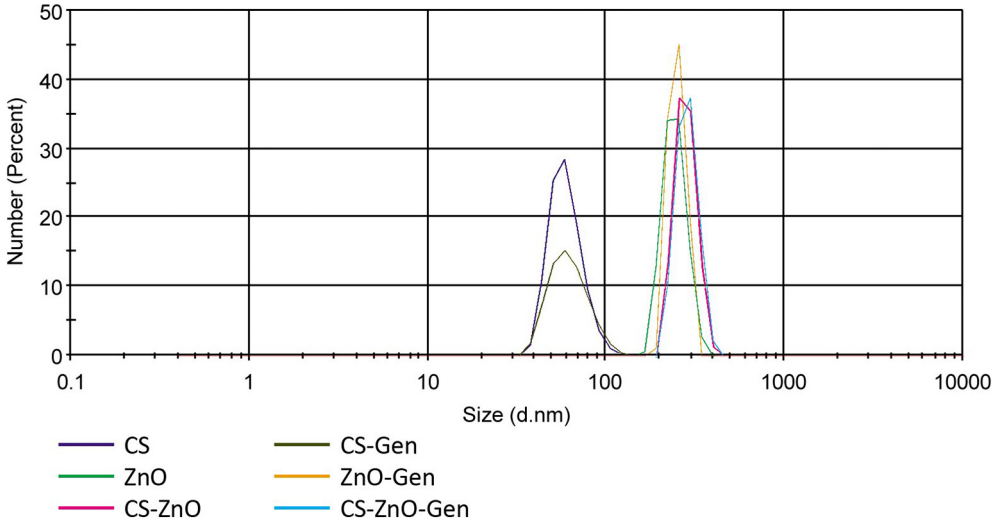

Fig. 1. Size distribution nanoparticles of chitosan (CS) and zinc oxide (ZnO) and chitosan-zinc oxide (CS-ZnO) nanocomposite.

3.2. Electron microscope images analysis

The size and morphology of the prepared NPs was studied by SEM. Due to Fig. 3, the CS NPs exhibited spherical morphology with mean diameter of 50–100 nm. Also, ZnO NPs showed rod morphology with mean diameter of 24–34 nm. After coating ZnO NPs with CS, rod shaped ZnO NPs were coated with spherical CS, in which the whole size became 33–49 nm.

3.3. FTIR spectroscopy

The FTIR spectrum of CS and ZnO NPs and CS-ZnO nanocomposite with/without gentamicin were presented in Fig. 4. As shown in the infrared spectrum of CS, characteristic peak at 3474 cm^{-1} can be attributed to the $-NH_2$ and –OH groups, the presence of a peak at 1732 cm^{-1}, demonstrating that the linkage between the phosphate groups of TPP and ammonium ions of chitosan. The sorption of gentamicin formed gentamicin-loaded CS. The peak at 3474 cm^{-1} ($-NH_2$ and –OH groups) in the spectrum of gentamicin-loaded NPs were shifted to 3442 cm^{-1} and became sharper.

In the FTIR spectrum of ZnO NPs, the strong adsorption bands observed at 417 cm^{-1}, which was related to the characteristic adsorption of ZnO. The broad peak at 2925 cm^{-1} can be attributed to the –OH groups of the adsorbed water molecules. Other peaks in the lower wavenumbers 1348, 1560, 1509, and 1043 cm^{-1} correspond to the carbonates in the sample. Also, the gentamicin loaded from the ZnO NPs was checked by FTIR spectroscopy. The vibration mode of alkyl C—H stretch, amine N—H stretch, and O—H stretch observed in the 2924–3422 cm^{-1}. NH_3^+ and NH_2^+ symmetric bend were observed at 1627 and 1508 cm^{-1} with lower energy than free gentamicin (1637 and 1533 cm^{-1}), demonstrating an interaction between ZnO and these moieties. The small intensity of Zn—O vibration compared to gentamicin characteristic vibration could demonstrate a high load of gentamicin into the NPs.

In CS-ZnO nanocomposite, a new broad adsorption peak at the 400–500 cm^{-1} was observed, which ascribed to the vibration of O—Zn—O groups. The characteristic peak at 3447 cm^{-1}, corresponding to the stretching vibration of –NH and –OH of CS was shifted to higher wavenumber 3450 cm^{-1} in CS-ZnO nanocomposite. The peak at 1732 cm^{-1} assigned to the bending vibration of–NH group present in CS, was shifted to lower wavenumber 1646 cm^{-1} in the CS-ZnO nanocomposite. Similar phenomena were observed with the peaks of C═O, 3′-OH, and 5′-OH groups. The reason for the above phenomena was the formation of hydrogen bands between ZnO and CS. The position of ZnO diffraction peaks; hence the inter planer spacing was slightly shifted. This shift is attributed to the reaction of ZnO with CS. The peak at 3450 cm^{-1} ($-NH_2$ and –OH groups) in the spectrum of gentamicin-loaded NPs was sharper and separately shifted to 3419 cm^{-1}.

3.4. X-ray diffraction (XRD) pattern of nanoparticles

The XRD plot of CS NPs, ZnO NPs, and CS-ZnO nanocomposite are presented in Fig. 5.

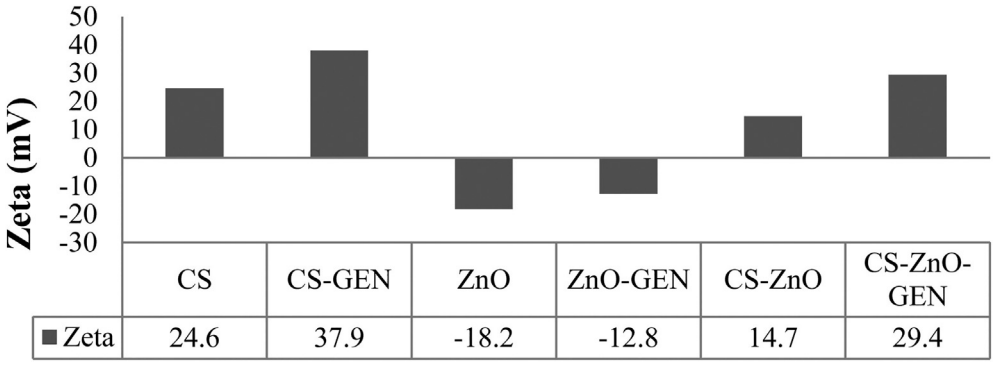

Fig. 2. Effect of gentamicin (GEN) on nanoparticles zeta potential of chitosan (CS), zinc oxide (ZnO) and chitosan-zinc oxide nanocomposite (CS-ZnO).

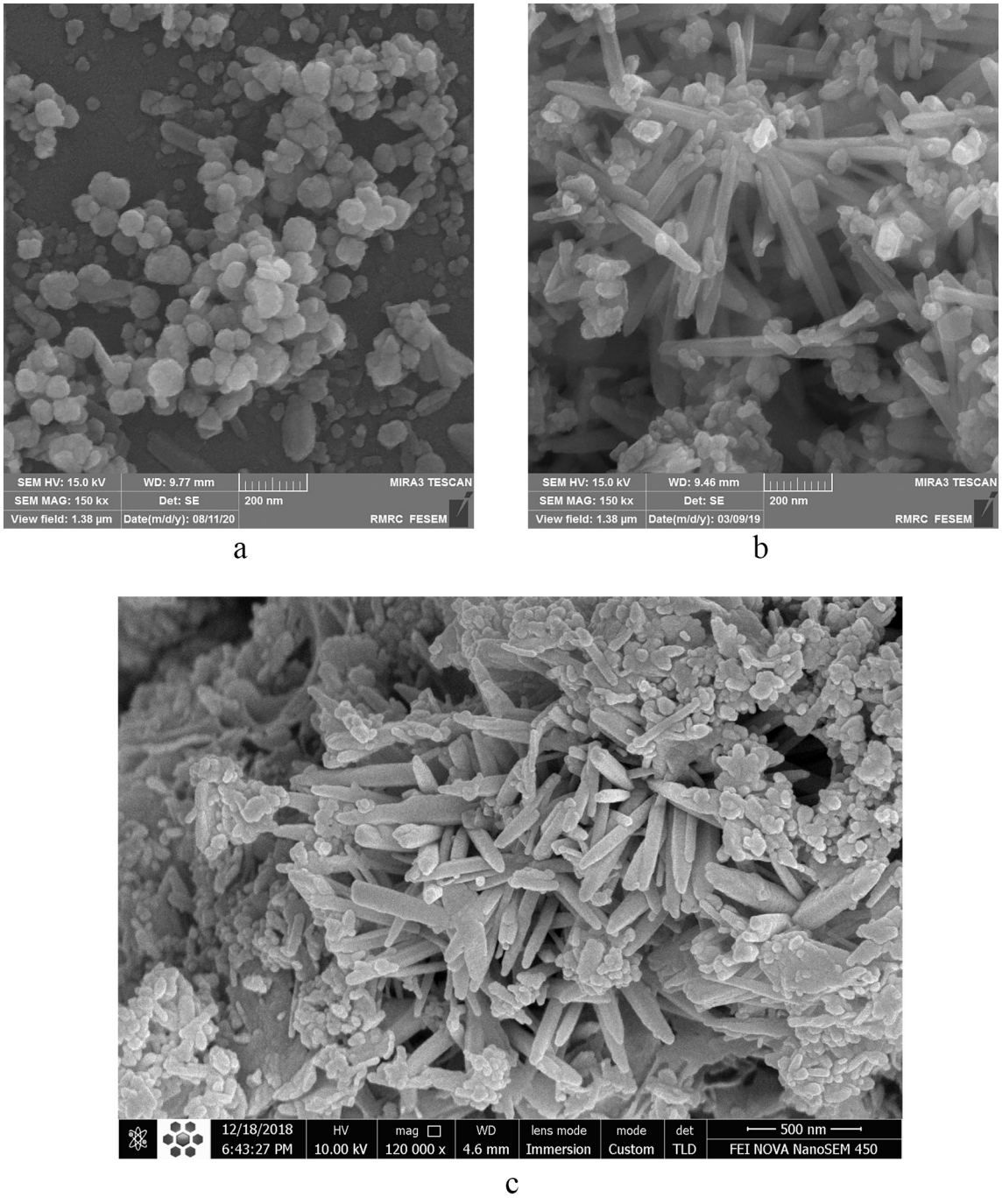

Fig. 3. SEM micrograph of chitosan nanoparticles (a), zinc oxide nanoparticles (b), chitosan-zinc oxide nanocomposite (c).

CS NPs shows two board characteristic peaks at $2\theta = 10.5°$ and $2\theta = 20.59°$. These two peaks corresponded to CS NPs hydrated crystalline structure. ZnO NPs showed the peaks at $2\theta = 31.9°$ (100), 34.5° (002), 36.4° (101), 47.8° (102), 56.9° (110), 62.8° (103), and 67.7° (112) corresponding to the hexagonal wurtzite structure of ZnO NPs (JCPDC card No 36-1459). The XRD profile of ZnO-CS nanocomposite indicated the key peaks corresponding to CS and ZnO NPs; nevertheless, in comparison with pure CS and ZnO NPs the intensity of CS-ZnO nanocomposite peaks was lower, this may be due to the interaction between CS and ZnO NPs functionalities. The XRD pattern of CS-ZnO nanocomposite demonstrated that the crystalline ZnO NPs structure was preserved even after the contact with CS. The presence of two sets of diffraction bound corresponding to ZnO and CS NPs confirms the prosperous creation of CS-ZnO nanocomposite

3.5. Drug entrapment and release of gentamicin from nanoparticles

The standard curve of gentamicin was presented in Fig. 6, where the scattered dots demonstrated the experimental data, and the blue line demonstrated the regression equation:

$$Y = 0.0134X - 0.2971$$

$$\left(R^2 = 0.9989\right)$$

where Y demonstrates the absorbance of nanoparticle dissolution at 400 nm; X demonstrates the gentamicin concentration, and R^2 is the associated factors. 0.9989 of R^2 value indicates that the regression equation matched well with the experimental data, and the equation can

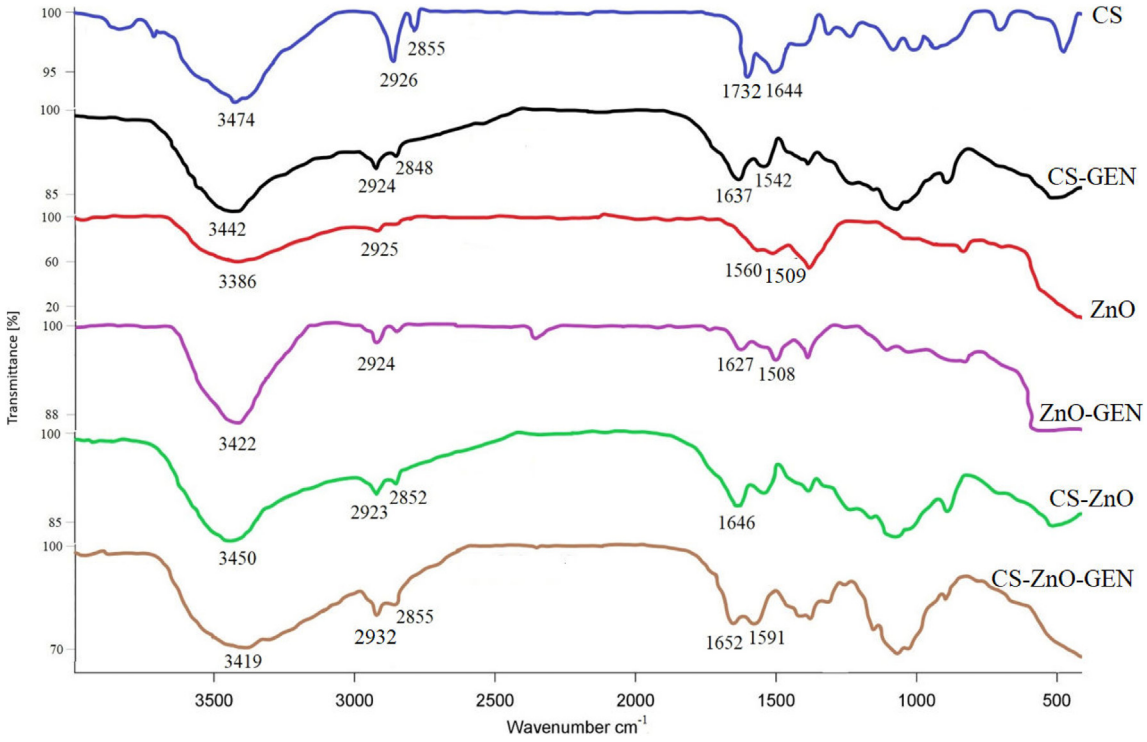

Fig. 4. Fourier transform infrared (FTIR) of nanoparticles of chitosan (CS), zinc oxide nanoparticles (ZnO), chitosan-zinc oxide (CS-ZnO) nanocomposite, chitosan-gentamicin (CS-GEN), zinc oxide-gentamicin (ZnO-GEN) and chitosan-zinc oxide-gentamicin (CS-ZnO-GEN).

be used to evaluate the number of drugs. Due to the standard curve and formula mentioned above, drug entrapment values with NPs synthesized under the acceptable situation can be calculated as 95.6%, 58.4%, and 53.8% for CS NPs, ZnO NPs, and CS-ZnO nanocomposite, respectively.

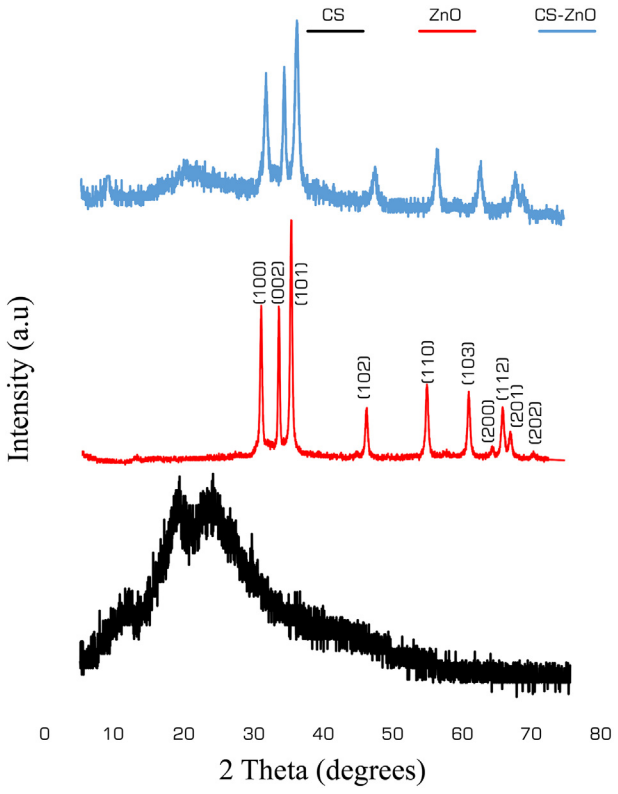

Fig. 5. XRD pattern of the nanoparticles of chitosan (CS) and zinc oxide (ZnO) and chitosan-zinc oxide (CS-ZnO) nanocomposite.

The release of gentamicin from gentamicin-loaded CS and ZnO NPs formulations provided a diphasic profile were determined with an initial burst release during the first 2 h, provided by a sustainable release profile. Around 90–95% of the gentamicin was released from NPs after first 2 h. The initial burst release may be ascribed to the distribution of gentamicin molecules which are localized near the surface of NPs. In other words, the gentamicin is lightly bound to the surface of NPs distributes out into the water-phase. The release of gentamicin from the gentamicin-loaded CS-ZnO nanocomposite was almost complete after 8 h. After 8 h, 88% of gentamicin amounts were released. The release curve was demonstrated in Fig. 7.

3.6. Antibacterial studies

The qualitative screening with the filter paper saturated at a concentration of 20 μL of stock solution (10 mg/mL) was effective against bacteria. The results obtained with the qualitative assay indicated that the growth inhibition zone is drastically increased by adding the active antibiotic compared to NPs alone. CS-ZnO-gentamicin nanocomposite increased the growth inhibition zone from 13.8 to 18.6 mm for *P. aeruginosa* PAO1 and 14.2 to 21.8 mm for *S. aureus* compared to CS-ZnO nanocomposite. The results showed that CS-ZnO-gentamicin nanocomposite has an increased growth inhibition zone of 12.9% and 16% for *P. aeruginosa* PAO1 and *S. aureus* compared to gentamicin alone, respectively. The experimental results are shown in Figs. 8 and 9.

The MIC assay indicated that CS-ZnO-gentamicin nanocomposite inhibited both *S. aureus* and *P. aeruginosa* PAO1 growth at much lower concentrations than nanocomposite alone. For *P. aeruginosa* PAO1, CS-ZnO-gentamicin MIC value was declined from 128 μg/mL to 0.5 μg/mL, while for *S. aureus*, MIC value was declined from 64 μg/mL to 0.125 μg/mL. The results are shown in Fig. 10. The results also proved that CS-ZnO-gentamicin nanocomposite had a four-fold MIC reduction in *S. aureus* and *P. aeruginosa* PAO1 compared to gentamicin alone.

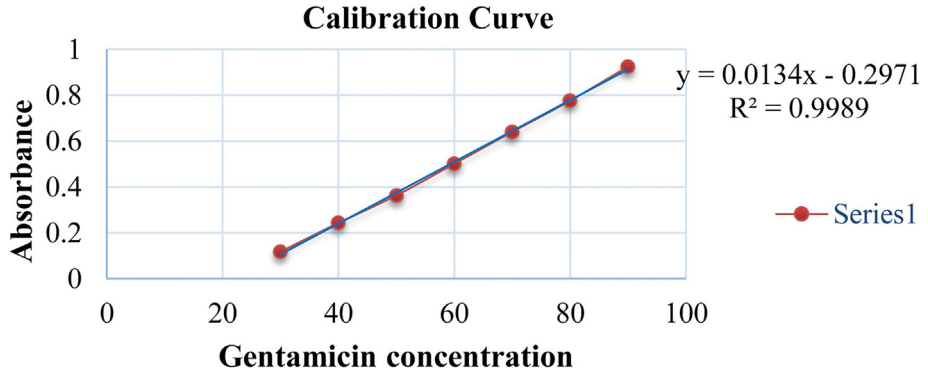

Fig. 6. Standard curve of gentamicin.

3.7. Effect on biofilm formation

CS and ZnO NPs and CS-ZnO nanocomposite with/without gentamicin were tested in the concentrations of 1/4 MIC and MIC range against both *P. aeruginosa* PAO1 and *S. aureus* biofilms (Fig. 11). A significant reduction in biofilm development was observed, when bacterial strains were treated with 1/4 MIC and MIC of all chemical components ($P < 0.05$). The concentration of MICs (128 μg/mL for *P. aeruginosa* PAO1 and 64 μg/mL for *S. aureus*) of CS-ZnO nanocomposite had a great biofilm decline of 63% and 67% for *P. aeruginosa* PAO1 and *S. aureus*, respectively. CS-ZnO nanocomposite with gentamicin in the concentration of MIC (0.5 and 0.125 μg/mL for *P. aeruginosa* PAO1 and *S. aureus*, respectively) was drastically decreased the biofilm formation of 84% and 77%, respectively. Furthermore, CS-ZnO nanocomposite with gentamicin was shown the great antibiofilm activity against *P. aeruginosa* PAO1 and *S. aureus* compared to gentamicin alone ($P < 0.05$). As the results showed, CS-ZnO nanocomposite had great antibiofilm activity than CS and ZnO NPs, so we selected CS-ZnO for cell viability studies.

3.8. Cytotoxicity assay results

Biocompatibility and nontoxicity are essential for NPs which used in the clinical antimicrobial and antibiofilm applications. Therefore, the toxicity of CS-ZnO nanocomposite for different concentrations was evaluated using HFFF2 cells by MTT assay. The cell viability of prepared CS-ZnO nanocomposite on HFFF2 cells was presented in Fig.12. Nanocomposite had no cytotoxic effects on HFFF2 cells in the effective bactericidal dose concentrations.

4. Discussion

P. aeruginosa and *S. aureus* are important opportunistic pathogens which are the most common pathogens causing biofilm-related infections in the human [36,37]. The inhibition of biofilm formation of these bacteria is among the most important strategies to control infections [34]. The main goal of this work was to synthesize CS-ZnO-gentamicin nanocomposite and assess antibiofilm activity on *P. aeruginosa* and *S. aureus*. The nanoparticles of CS, ZnO, and CS-ZnO nanocomposite were synthesized with the simple ionic cross-linking using TPP, conventional heating, and chemical precipitation technique, respectively. Then, the gentamicin was loaded on freshly prepared nanoparticles of CS and ZnO. At the same time, for the synthesis of CS-ZnO-gentamicin nanocomposite, we incorporated gentamicin coated ZnO nanoparticles into CS solution to obtain a hybrid inorganic-organic material (the ratio of CS to ZnO was 1:1). The synthesized CS-ZnO nanocomposite morphology was the combination of nanospheres and nanorods with size distributions of 277.5 nm and positive surface charge (+14.7 mV). While, after gentamicin loading on nanocomposite, its size and zeta potential was changed to 284.5 nm and +29.4 mV respectively.

The effect of different natural and synthetic compounds on biofilm formation in selected bacteria was investigated [38]. Several researches showed that the NPs of CS and ZnO had great antibacterial and antibiofilm activities in planktonic and biofilm forms of bacteria [19,39,40]. The synergistic activity of CS and ZnO NPs and CS-ZnO nanocomposite with gentamicin was evaluated on the growth and biofilm formation of *P. aeruginosa* PAO1 and *S. aureus*. Due to our results, gentamicin-loaded NPs demonstrated increased antibacterial activity on these bacteria compared to the gentamicin. The present study is in close agreement with previous studies in antibacterial activity by NPs such as ZnO NP and gentamicin-loaded ZnO NPs against the

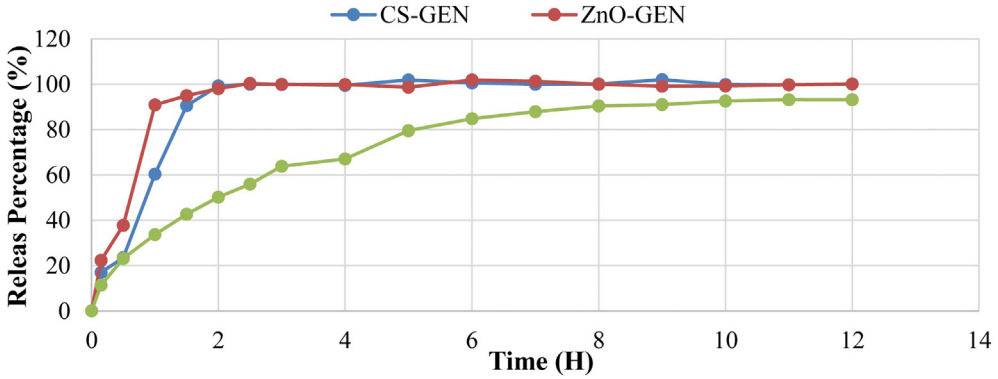

Fig. 7. The gentamicin (GEN) release from the nanoparticles of chitosan (CS), zinc oxide (ZnO) and chitosan-zinc oxide (CS-ZnO) nanocomposite.

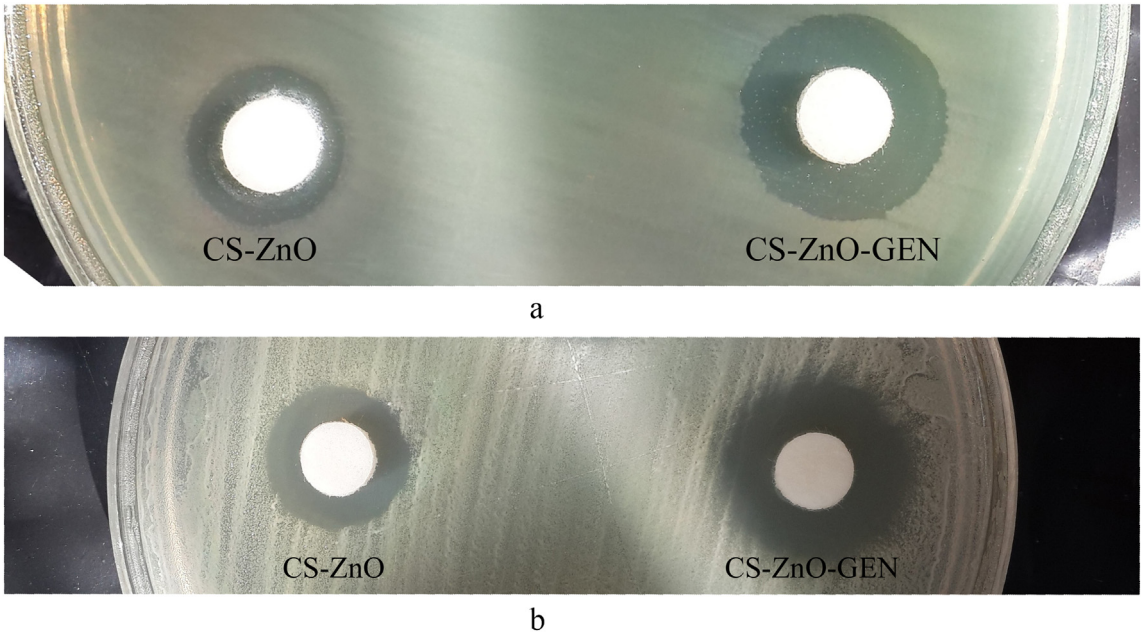

Fig. 8. Antibacterial activities of chitosan-zinc oxide nanocomposite (A) and chitosan-zinc oxide-gentamicin nanocomposite (B) on *P. aeruginosa* PAO1 (a) and *S. aureus* (b) culture.

P. aeruginosa and *S. aureus* [20]. Besides, a similar result was obtained in the ZnO/gentamicin-CS composite, in which the composite inhibits the growth of *P. aeruginosa* and *S. aureus* [19]. To determine the antibacterial efficiency of NPs with/without gentamicin against *P. aeruginosa* PAO1 and *S. aureus*, we investigated their possible antibiofilm activity in the concentration ranges of MIC and 1/4 MIC. Our findings showed that NPs with/without gentamicin drastically decrease biofilm formation of *P. aeruginosa* PAO1 and *S. aureus*. In this regard, several studies were conducted; Lee et al. demonstrated that Zn^{2+} and ZnO NPs had no bactericidal activity against *P. aeruginosa* in the concentration levels of <3 mM, surprisingly they had the antibiofilm activity [41], which is contributed to the generation of reactive oxygen species (ROS) on the surface of ZnO which could induce serious damage on bacterial cells. Also, the attachment of ZnO NPs on the bacterial surface or cumulating of NPs in the cytoplasm area induces the disturbance of cellular action and destruction of the bacterial membrane [42,43]. Lara et al. reported that ZnO NPs could significantly reduce biofilm-production in *P. aeruginosa*, demonstrating that ZnO NPs have a wide spectrum and maybe an alternative option for the treatment of *P. aeruginosa* infections [40].

Several studies showed that the sub-MIC concentrations of CS NPs and silver nanowires could inhibit bacterial biofilm formation [44,45]. There is a layer of anionic-charged lipopolysaccharide with poor strength and sustainability at the outer membrane of *P. aeruginosa*. Therefore, the lipopolysaccharides can be attached to the amino groups of CS NPs with cationic-charged and afterward, fragmented. Thus, the CS NPs cause bacterial death with altering bacteria permeability via membrane integration. In *S. aureus*, the cell wall is composed of the several layers of peptidoglycan which reduces the permeability of CS NPs [46,47]. Due to the results obtained by Lin et al., gentamicin-loaded nanotubes titanium could significantly inhibit bacterial adhesion and biofilm development in comparison to Flat titanium and/or nanotubes with no drug loading in *S. aureus* and *Staphylococcus epidermidis* [48]. Studies reported that iron NPs (FeOOH NPs) and gentamicin-loaded gold (Au) NPs inhibited *P. aeruginosa* biofilm at the initial attachment phase and maturation phase of biofilm development, respectively

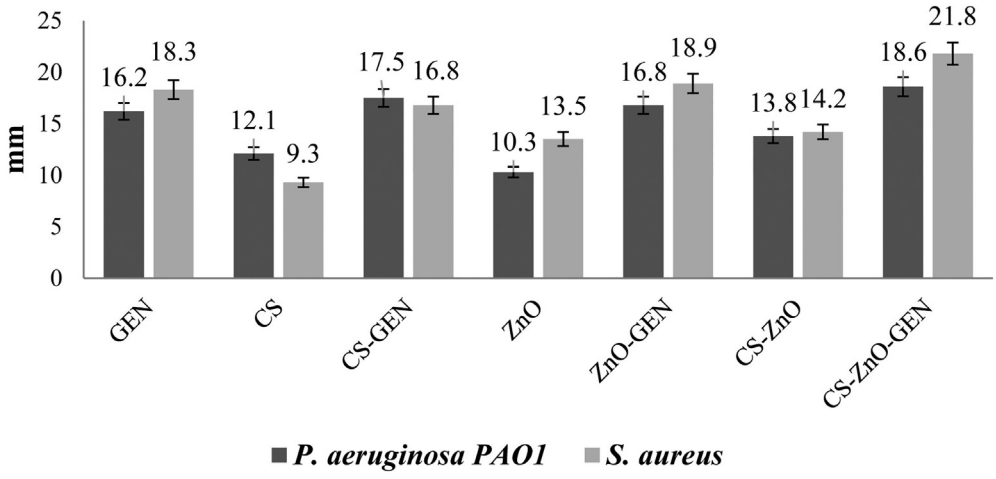

Fig. 9. Measured growth inhibition zone (mm) of chitosan nanoparticles (CS), zinc oxide nanoparticles (ZnO), and chitosan-zinc oxide nanocomposite (CS-ZnO) in combination with/without gentamicin (GEN) against *P. aeruginosa* PAO1 and *S. aureus*.

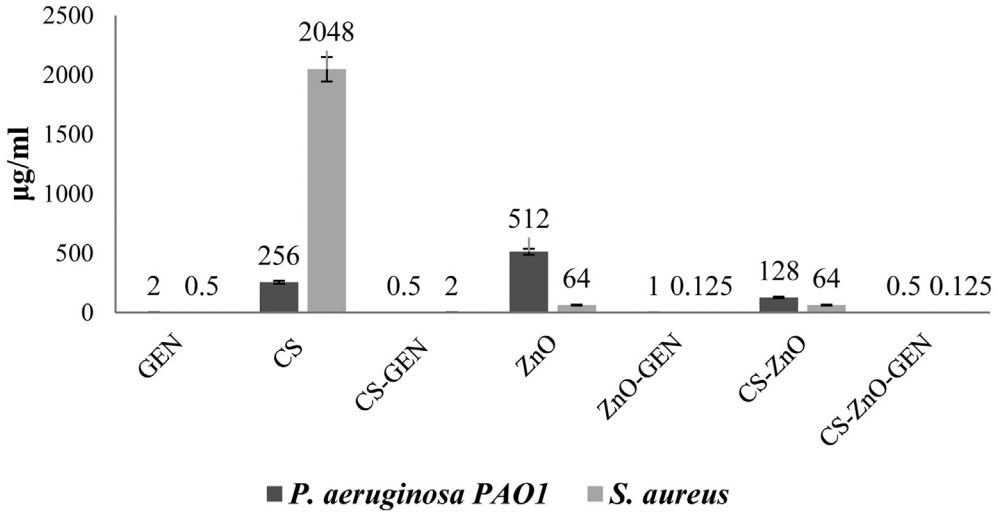

Fig. 10. Minimum inhibition concentration (MIC) of nanoparticle of chitosan (CS), zinc oxide and chitosan-zinc oxide (CS-ZnO) nanocomposite in combination with/without gentamicin (GEN) against *P. aeruginosa* PAO1 and *S. aureus*.

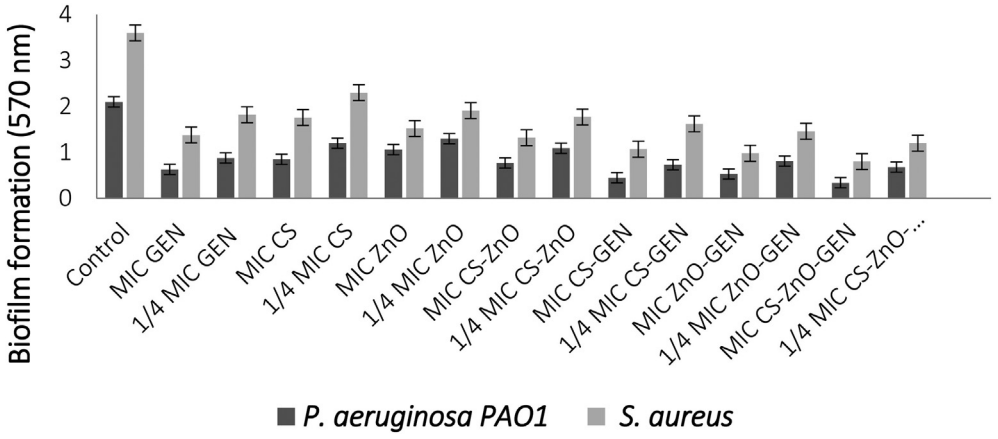

Fig. 11. Effect of nanoparticles of chitosan (CS), zinc-oxide (ZnO) and chitosan-zinc oxide (CS-ZnO) nanocomposite in combination with/without gentamicin (GEN) at concentrations 1/4 MIC and MIC on biofilm development of *P. aeruginosa* PAO1 and *S. aureus* $P < 0.05$.

[49,50]. NPs of ZnO and CS decrease bacterial attachment, replication, and biofilm development due to their robust antibacterial activity [45]. Huang et al. reported that the metabolic activity and secretion of exopolysaccharide in the biofilms of *Escherichia coli* and *S. aureus* was significantly diminished after the treatment of sulfonated CS [51].

P. aeruginosa PAO1 and *S. aureus* produce extracellular polymeric substances (EPS) which play a vital role in the primary bacterial attachment to the surface of host cells and in developing an intricate biofilm structure which resulted in difficult treatment management with the host immune system and classical antibiotics [36,37]. EPS is one of the

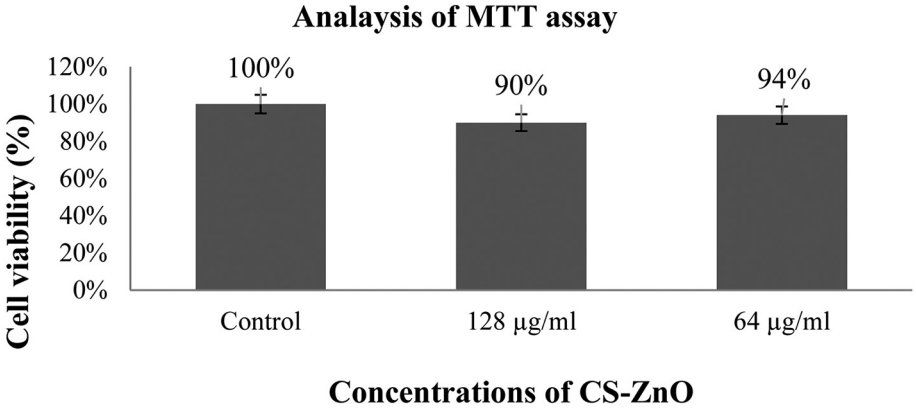

Fig. 12. Cytotoxicity effects of chitosan-zinc oxide nanocomposite (CS-ZnO) on HFFF2 cells. Cells without nanocomposite were used as a control.

key strategies of bacteria for antibiotic resistance. Moreover, EPS reduction is regarded as one of the mains restrictive of biofilm development [52]. The antibiofilm effect of NPs can be due to the inhibition of EPS development which proved that NPs disrupt EPS production, thereby reducing biofilm formation [17,53].

Kalishwaralal et al. [54] reported that inhibition of bacterial biofilms with NPs could be due to the creation of several water channels in the biofilm. The bacteria use these pores to transport nutrients; therefore, NPs can spread from these channels and perform as an antibacterial agent in biofilm. Another possible mechanism for the antibiofilm activity of NPs is related to the inhibition of efflux pumps [55]. Gupta et al. showed the effective role of efflux pumps in developing the biofilm and the expression of efflux pumps is revealed to be directly regulated in biofilms which increases antibiotic resistance [55]. Besides, Padwal et al. [56] indicated NPs with antibiotics act as efflux pump inhibitors. They suggested that NPs can inhibit efflux pumps through binding to the active site of efflux pumps, block the extrusion of antibiotics outside the cells and distract efflux kinetics. They have already been discovered the inhibitory effect of ZnO NPs on NorA and MexAM-OPrM efflux pumps of *S. aureus* and *P. aeruginosa*, respectively [57,58]. Due to these researches, the inhibition or down-regulation of efflux pumps with NPs could provide a hopeful method to decelerate and/or inhibit the biofilm formation of bacterial pathogens.

5. Conclusions

CS-ZnO nanocomposite was synthesized with a simple chemical precipitation method with a particle size of 277.5 nm and a surface charge of +14.7 mV. Cytotoxicity of CS-ZnO nanocomposite was determined with the MTT assay. The results showed that CS-ZnO nanocomposite had no cytotoxic effects on HFFF2 cells in the effective bactericidal dose concentrations. The incorporation of gentamicin loaded ZnO nanoparticles in CS solution showed slow release rate of drug compared to gentamicin loaded ZnO and CS nanoparticles. As all three components (gentamicine alone, ZnO NPs, and CS NPs) showed the antibacterial and antibiofilm activity, while the highest antibacterial and antibiofilm activity was observed in gentamicin loaded CS-ZnO nanocomposite due to the synergistic action of gentamicin and CS-ZnO nanocomposite. The results proved a four-fold MIC reduction in *S. aureus* and *P. aeruginosa* PAO1 compared to gentamicin alone as well as 84% reduction of biofilm formation for *P. aeruginosa* PAO1 and 77% reduction of biofilm formation for *S. aureus*. Therefore, these combinations can lead to developing the new combined therapy against *P. aeruginosa* and *S. aureus* biofilm-related infections.

CRediT authorship contribution statement

Fatemeh Hemmati: Conceptualization, Data curation, Formal analysis, Investigation, Methodology, Software, Validation, Visualization, Writing - original draft, Writing - review & editing. **Roya Salehi:** Data curation, Formal analysis, Methodology, Software, Validation, Visualization, Writing - review & editing. **Reza Ghotasluo:** Conceptualization, Formal analysis, Funding acquisition, Methodology, Project administration, Validation, Visualization, Writing - review & editing. **Hossein Samadi Kafil:** Data curation, Formal analysis, Investigation, Methodology, Visualization, Writing - review & editing. **Alka Hasani:** Data curation, Formal analysis, Investigation, Methodology, Visualization, Writing - review & editing. **Pourya Gholizadeh:** Data curation, Formal analysis, Investigation, Methodology, Visualization, Writing - review & editing. **Mohammad Ahangarzadeh Rezaee:** Conceptualization, Funding acquisition, Investigation, Methodology, Project administration, Supervision, Validation, Visualization, Writing - review & editing.

Declaration of competing interest

The authors have reported no conflict of interest.

Acknowledgments

This work was financially supported by the Immunology Research Center, Tabriz University of Medical Sciences, Tabriz, Iran (Grant No. 97/60073).

References

[1] S. Dananjaya, R.S. Kumar, M. Yang, C. Nikapitiya, J. Lee, M. De Zoysa, Synthesis, characterization of ZnO-chitosan nanocomposites and evaluation of its antifungal activity against pathogenic *Candida albicans*, Int. J. Biol. Macromol. 108 (2018) 1281–1288.
[2] E. Galdiero, L. Lombardi, A. Falanga, G. Libralato, M. Guida, R. Carotenuto, Biofilms: novel strategies based on antimicrobial peptides, Pharmaceutics 11 (7) (2019) 322.
[3] S. Fulaz, S. Vitale, L. Quinn, E. Casey, Nanoparticle–biofilm interactions: the role of the EPS matrix, Trends Microbiol. 27 (11) (2019) 915–926.
[4] N. Talebian, H.S.H. Zavvare, Enhanced bactericidal action of SnO_2 nanostructures having different morphologies under visible light: influence of surfactant, J. Photochem. Photobiol. B 130 (2014) 132–139.
[5] G. Batoni, G. Maisetta, S. Esin, Antimicrobial peptides and their interaction with biofilms of medically relevant bacteria, BBA-Biomembranes 1858 (5) (2016) 1044–1060.
[6] A. Sanmugam, D. Vikraman, H.J. Park, H.-S. Kim, One-Pot facile methodology to synthesize chitosan-ZnO-graphene oxide hybrid composites for better dye adsorption and antibacterial activity, Nanomaterials 7 (11) (2017) 363.
[7] M. Karpuraranjith, S. Thambidurai, Chitosan/zinc oxide-polyvinylpyrrolidone (CS/ZnO-PVP) nanocomposite for better thermal and antibacterial activity, Int. J. Biol. Macromol. 104 (2017) 1753–1761.
[8] F. Wahid, J.-J. Yin, D.-D. Xue, H. Xue, Y.-S. Lu, C. Zhong, L.-Q. Chu, Synthesis and characterization of antibacterial carboxymethyl chitosan/ZnO nanocomposite hydrogels, Int. J. Biol. Macromol. 88 (2016) 273–279.
[9] N.A. Al-Tayyar, A.M. Youssef, R.R. Al-Hindi, Antimicrobial packaging efficiency of ZnO-SiO_2 nanocomposites infused into PVA/CS film for enhancing the shelf life of food products, Food Packag. Shelf Life 25 (2020), 100523, .
[10] P. Sahariah, V.S. Gaware, R. Lieder, S. Jónsdóttir, M.Á. Hjálmarsdóttir, O.E. Sigurjonsson, M. Másson, The effect of substituent, degree of acetylation and positioning of the cationic charge on the antibacterial activity of quaternary chitosan derivatives, Mar. Drugs 12 (8) (2014) 4635–4658.
[11] K.A. O'Callaghan, J.P. Kerry, Preparation of low-and medium-molecular weight chitosan nanoparticles and their antimicrobial evaluation against a panel of microorganisms, including cheese-derived cultures, Food Control 69 (2016) 256–261.
[12] M. Premanathan, K. Karthikeyan, K. Jeyasubramanian, G. Manivannan, Selective toxicity of ZnO nanoparticles toward Gram-positive bacteria and cancer cells by apoptosis through lipid peroxidation, Nanomed-Nanotechnol 7 (2) (2011) 184–192.
[13] N.A. Al-Tayyar, A.M. Youssef, R. Al-Hindi, Antimicrobial food packaging based on sustainable bio-based materials for reducing foodborne pathogens: a review, Food Chem. 310 (2020), 125915, .
[14] E. Wenzig, U. Widowitz, O. Kunert, S. Chrubasik, F. Bucar, E. Knauder, R. Bauer, Phytochemical composition and in vitro pharmacological activity of two rose hip (Rosa canina L.) preparations, Phytomedicine 15 (10) (2008) 826–835.
[15] S.M. El-Sayed, H.S. El-Sayed, O.A. Ibrahim, A.M. Youssef, Rational design of chitosan/guar gum/zinc oxide bionanocomposites based on Roselle calyx extract for Ras cheese coating, Carbohydr. Polym. 239 (2020), 116234, .
[16] P.P. Mahamuni-Badiger, P.M. Patil, M.V. Badiger, P.R. Patel, B.S. Thorat-Gadgil, A. Pandit, R.A. Bohara, Biofilm formation to inhibition: role of zinc oxide-based nanoparticles, Mater. Sci. Eng. C 108 (2020), 110319, .
[17] A.-S.A. Al-Sherbini, H.E. Ghannam, G.M. El-Ghanam, A.A. El-Ella, A.M. Youssef, Utilization of chitosan/Ag bionanocomposites as eco-friendly photocatalytic reactor for bactericidal effect and heavy metals removal, Heliyon 5 (6) (2019), e01980, .
[18] B.S. Vasile, O. Oprea, G. Voicu, A. Ficai, E. Andronescu, A. Teodorescu, A. Holban, Synthesis and characterization of a novel controlled release zinc oxide/gentamicin–chitosan composite with potential applications in wounds care, Int. J. Pharm. 463 (2) (2014) 161–169.
[19] G. Voicu, O. Oprea, B. Vasile, E. Andronescu, Antibacterial activity of zinc oxide-gentamicin hybrid material, Dig. J. Nanomater. Biostruct. 8 (3) (2013).
[20] M.-P. Mingeot-Leclercq, Y. Glupczynski, P.M. Tulkens, Aminoglycosides: activity and resistance, Antimicrob. Agents Chemother. 43 (4) (1999) 727–737.
[21] P. Dozzo, H.E. Moser, New aminoglycoside antibiotics, Exp. Opin. Ther. Pat. 20 (10) (2010) 1321–1341.
[22] M. Schroeder, B.D. Brooks, A.E. Brooks, The complex relationship between virulence and antibiotic resistance, Genes 8 (1) (2017) 39.
[23] Y. Morita, J. Tomida, Y. Kawamura, Responses of *Pseudomonas aeruginosa* to antimicrobials, Front. Microbiol. 4 (2014) 422.
[24] N. Talebian, S.M. Amininezhad, M. Doudi, Controllable synthesis of ZnO nanoparticles and their morphology-dependent antibacterial and optical properties, J. Photochem. Photobiol. B 120 (2013) 66–73.
[25] A. Anitha, V.D. Rani, R. Krishna, V. Sreeja, N. Selvamurugan, S. Nair, H. Tamura, R. Jayakumar, Synthesis, characterization, cytotoxicity and antibacterial studies of chitosan, O-carboxymethyl and N,O-carboxymethyl chitosan nanoparticles, Carbohydr. Polym. 78 (4) (2009) 672–677.
[26] V. Kamat, D. Bodas, K. Paknikar, Chitosan nanoparticles synthesis caught in action using microdroplet reactions, Sci. Rep. 6 (1) (2016) 1–4.

[27] S. Jafarirad, M. Mehrabi, B. Divband, M. Kosari-Nasab, Biofabrication of zinc oxide nanoparticles using fruit extract of Rosa canina and their toxic potential against bacteria: a mechanistic approach, Mater. Sci. Eng. C 59 (2016) 296–302.
[28] S.E.-S. Saeed, M.M. El-Molla, M.L. Hassan, E. Bakir, M.M. Abdel-Mottaleb, M.S. Abdel-Mottaleb, Novel chitosan-ZnO based nanocomposites as luminescent tags for cellulosic materials, Carbohydr. Polym. 99 (2014) 817–824.
[29] P. Frutos, S. Torrado, M. Perez-Lorenzo, G. Frutos, A validated quantitative colorimetric assay for gentamicin, J. Pharm. Biomed. 21 (6) (2000) 1149–1159.
[30] J. Guan, P. Cheng, S. Huang, J. Wu, Z. Li, X. You, L. Hao, Y. Guo, R. Li, H. Zhang, Optimized preparation of levofloxacin-loaded chitosan nanoparticles by ionotropic gelation, Phys. Procedia 22 (2011) 163–169.
[31] Y.-C. Huang, R.-Y. Li, J.-Y. Chen, J.-K. Chen, Biphasic release of gentamicin from chitosan/fucoidan nanoparticles for pulmonary delivery, Carbohydr. Polym. 138 (2016) 114–122.
[32] M. Laurenti, V. Cauda, Gentamicin-releasing mesoporous zno structures, Materials 11 (2) (2018) 314.
[33] A.M. Grumezescu, E. Andronescu, A. Ficai, C. Bleotu, M.C. Chifiriuc, Chitin based biomaterial for antimicrobial therapy: fabrication, characterization and in vitro profile based interaction with eukaryotic and prokaryotic cells, Biointerface Res. Appl. Chem. 2 (5) (2012).
[34] S. El-Mowafy, M. Shaaban, K. Abd El Galil, Sodium ascorbate as a quorum sensing inhibitor of *Pseudomonas aeruginosa*, J. Appl. Microbiol. 117 (5) (2014) 1388–1399.
[35] J. Xu, Y. Zhang, Y. Gutha, W. Zhang, Antibacterial property and biocompatibility of chitosan/poly (vinyl alcohol)/ZnO (CS/PVA/ZnO) beads as an efficient adsorbent for Cu (II) removal from aqueous solution, Colloids Surf. B 156 (2017) 340–348.
[36] F. Khan, J.-W. Lee, P. Manivasagan, D.T.N. Pham, J. Oh, Y.-M. Kim, Synthesis and characterization of chitosan oligosaccharide-capped gold nanoparticles as an effective antibiofilm drug against the *Pseudomonas aeruginosa* PAO1, Microb. Pathog. 135 (2019), 103623, .
[37] V. Pérez-Laguna, I. García-Luque, S. Ballesta, L. Pérez-Artiaga, V. Lampaya-Pérez, S. Samper, P. Soria-Lozano, A. Rezusta, Y. Gilaberte, Antimicrobial photodynamic activity of Rose Bengal, alone or in combination with Gentamicin, against planktonic and biofilm *Staphylococcus aureus*, Photodiagn. Photodyn. Ther. 21 (2018) 211–216.
[38] S.A. El-Mowafy, K.H. Abd El Galil, S.M. El-Messery, M.I. Shaaban, Aspirin is an efficient inhibitor of quorum sensing, virulence and toxins in *Pseudomonas aeruginosa*, Microb. Pathog. 74 (2014) 25–32.
[39] S. Ilk, N. Sağlam, M. Özgen, F. Korkusuz, Chitosan nanoparticles enhances the anti-quorum sensing activity of kaempferol, Int. J. Biol. Macromol. 94 (2017) 653–662.
[40] B. García-Lara, M. Saucedo-Mora, J. Roldán-Sánchez, B. Pérez-Eretza, M. Ramasamy, J. Lee, R. Coria-Jimenez, M. Tapia, V. Varela-Guerrero, R. García-Contreras, Inhibition of quorum-sensing-dependent virulence factors and biofilm formation of clinical and environmental *Pseudomonas aeruginosa* strains by ZnO nanoparticles, Lett. Appl. Microbiol. 61 (3) (2015) 299–305.
[41] J.-H. Lee, Y.-G. Kim, M.H. Cho, J. Lee, ZnO nanoparticles inhibit *Pseudomonas aeruginosa* biofilm formation and virulence factor production, Microbiol. Res. 169 (12) (2014) 888–896.
[42] L. Zhang, Y. Jiang, Y. Ding, N. Daskalakis, L. Jeuken, M. Povey, A.J. O'Neill, D.W. York, Mechanistic investigation into antibacterial behaviour of suspensions of ZnO nanoparticles against *E. coli*, J. Nanopart. Res. 12 (5) (2010) 1625–1636.
[43] L. Zhang, Y. Jiang, Y. Ding, M. Povey, D. York, Investigation into the antibacterial behaviour of suspensions of ZnO nanoparticles (ZnO nanofluids), J. Nanopart. Res. 9 (3) (2007) 479–489.
[44] S.N. Muslim, I.M.A. Kadmy, A.N.M. Ali, B.K. Salman, M. Ahmad, S.S. Khazaal, N.H. Hussein, S.N. Muslim, Chitosan extracted from Aspergillus flavus shows synergistic effect, eases quorum sensing mediated virulence factors and biofilm against nosocomial pathogen *Pseudomonas aeruginosa*, Int. J. Biol. Macromol. 107 ((2018) 52–58.
[45] M.S. Wagh, R.H. Patil, D.K. Thombre, M.V. Kulkarni, W.N. Gade, B.B. Kale, Evaluation of anti-quorum sensing activity of silver nanowires, Appl. Microbiol. Biotechnol. 97 (8) (2013) 3593–3601.
[46] G. Gedda, S. Pandey, Y.-C. Lin, H.-F. Wu, Antibacterial effect of calcium oxide nanoplates fabricated from shrimp shells, Green Chem. 17 (6) (2015) 3276–3280.
[47] A. Jordan, A. Haiß, M. Spulak, Y. Karpichev, K. Kümmerer, N. Gathergood, Synthesis of a series of amino acid derived ionic liquids and tertiary amines: green chemistry metrics including microbial toxicity and preliminary biodegradation data analysis, Green Chem. 18 (16) (2016) 4374–4392.
[48] W.-t. Lin, H.-l. Tan, Z.-l. Duan, B. Yue, R. Ma, G. He, T.-t. Tang, Inhibited bacterial biofilm formation and improved osteogenic activity on gentamicin-loaded titania nanotubes with various diameters, Int. J. Nanomedicine 9 (2014) 1215.
[49] D.T.N. Pham, F. Khan, T.T.V. Phan, S.-k. Park, P. Manivasagan, J. Oh, Y.-M. Kim, Biofilm inhibition, modulation of virulence and motility properties by FeOOH nanoparticle in *Pseudomonas aeruginosa*, Braz. J. Microbiol. 50 (3) (2019) 791–805.
[50] H. Mu, J. Tang, Q. Liu, C. Sun, T. Wang, J. Duan, Potent antibacterial nanoparticles against biofilm and intracellular bacteria, Sci. Rep. 6 (1) (2016) 1–9.
[51] J. Huang, Y. Liu, L. Yang, F. Zhou, Synthesis of sulfonated chitosan and its antibiofilm formation activity against *E. coli* and *S. aureus*, Int. J. Biol. Macromol. 129 (2019) 980–988.
[52] P. Bhattacharyya, B. Agarwal, M. Goswami, D. Maiti, S. Baruah, P. Tribedi, Zinc oxide nanoparticle inhibits the biofilm formation of *Streptococcus pneumoniae*, Antonie Van Leeuwenhoek 111 (1) (2018) 89–99.
[53] Z. Wang, H. Bai, C. Lu, C. Hou, Y. Qiu, P. Zhang, J. Duan, H. Mu, Light controllable chitosan micelles with ROS generation and essential oil release for the treatment of bacterial biofilm, Carbohydr. Polym. 205 (2019) 533–539.
[54] K. Kalishwaralal, S. BarathManiKanth, S.R.K. Pandian, V. Deepak, S. Gurunathan, Silver nanoparticles impede the biofilm formation by *Pseudomonas aeruginosa* and *Staphylococcus epidermidis*, Colloids Surf B 79 (2) (2010) 340–344.
[55] D. Gupta, A. Singh, A.U. Khan, Nanoparticles as efflux pump and biofilm inhibitor to rejuvenate bactericidal effect of conventional antibiotics, Nanoscale Res. Lett. 12 (1) (2017) 1–6.
[56] P. Padwal, R. Bandyopadhyaya, S. Mehra, Polyacrylic acid-coated iron oxide nanoparticles for targeting drug resistance in mycobacteria, Langmuir 30 (50) (2014) 15266–15276.
[57] M. Banoee, S. Seif, Z.E. Nazari, P. Jafari-Fesharaki, H.R. Shahverdi, A. Moballegh, K.M. Moghaddam, A.R. Shahverdi, ZnO nanoparticles enhanced antibacterial activity of ciprofloxacin against *Staphylococcus aureus* and *Escherichia coli*, J. Biomed. Mater. Res. B 93 (2) (2010) 557–561.
[58] P.D. Nallathamby, K.J. Lee, T. Desai, X.-H.N. Xu, Study of the multidrug membrane transporter of single living *Pseudomonas aeruginosa* cells using size-dependent plasmonic nanoparticle optical probes, Biochemistry 49 (28) (2010) 5942–5953.